

Research Papers
Issue RP0247
December 2014

*Numerical Applications
and Scenarios (ANS)
Division, CMCC Bologna*

GLOB16, the CMCC global mesoscale-eddy ocean

By **Doroteaciro Iovino**
dorotea.iovino@cmcc.it

Andrea Storto

Simona Masina

Andrea Cipollone

and **Vladimir Stepanov**

SUMMARY This report presents the global ocean/sea ice configuration at eddy-resolving resolution developed at CMCC, and describes numerical results from the first simulation. The model configuration, based on the NEMO system, has $1/16^\circ$ horizontal spacing at the equator and uses 98 vertical levels. So far this is the highest resolution implemented in a global NEMO domain. The numerical experiment has been performed on the MareNostrum cluster located at the Barcelona Supercomputing Center (within the framework of the ENS4OCEAN project awarded in the PRACE 8th Regular Call). This simulation represents a major step forward in high resolution ocean modeling.

*We acknowledge PRACE
for awarding us access to
resource MareNostrum
based at the Barcelona
Supercomputing Center
(BSC-CNS) in Spain.*



02

Contents

| | |
|--|----|
| Contents | 2 |
| 1. Introduction | 3 |
| 2. The numerical code | 4 |
| Ocean physics | 5 |
| 3. Surface Boundary condition | 8 |
| Runoff | 8 |
| Surface restoring | 10 |
| 4. Model configuration | 10 |
| Grid | 10 |
| Bathymetry | 11 |
| Initial conditions | 12 |
| Running strategy | 12 |
| 5. Implementation of optimized collective IO for variable reconstruction | 12 |
| 6. Results | 15 |
| Bibliography | 21 |



1. INTRODUCTION

The global ocean is a highly turbulent system over a wide range of space and time scales. Both satellite and in situ data show that small-scale eddies, meanders, fronts and filaments pervade the ocean at all latitude bands, and the ocean circulation is indeed dominated by mesoscale variability. Mesoscale eddies usually account for the peak in the kinetic energy spectrum; most of their energy is generated and maintained by baroclinic instabilities of large-scale flows.

Those processes play a substantial role in the dynamics of the global ocean (e.g., transporting and mixing temperature and salinity, exchanging energy and momentum with the mean flow, controlling the mechanisms of spreading of deep waters, preconditioning of deep convection, modulate air-sea interactions [34]), but the dominant length-scale of these eddies varies greatly with latitude, stratification and ocean depth. Mesoscale eddies typically have horizontal scales of the order of the first baroclinic Rossby radius of deformation (varying roughly from 200km in the tropics to ~ 10 km in the subtropical region [8]), vertical scales ranging from the pycnocline depth to the full ocean depth and time scales of weeks and months. In the context of ocean models, the mesoscale is adequately described as long as the grid spacing is finer than the first baroclinic Rossby radius.

Global numerical ocean models, with spatial resolutions ranging from 1° down to only a few kilometers, often include both regions where the dominant eddy scales are well resolved and regions where the model resolution is too coarse for eddies to form and hence eddy effects have to be parameterized. A model will be *eddy rich* if it uses a horizontal grid mesh whose resolution is fine enough to let mesoscale dynamics emerge, i.e. baroclinic and barotropic instability processes are ex-

plicitly (albeit partially) resolved. Since the milestone paper by Smith et al. (2000) [36], mesoscale eddies are considered *resolved* in most oceanic regions when the horizontal grids are refined to $1/10^\circ$ at the equator. Such horizontal resolution adequately simulates, on Mercator grid, both mesoscale variability and narrow mean flows such as western boundary currents only for latitude regions equatorward of 50° . Resolving mesoscale eddy variability remains elusive in the high-latitudes due to the reduction of the baroclinic Rossby radius ([18]). In the Arctic Ocean, the first Rossby radius decreases down to ~ 10 km [31]. Typical eddy-resolving resolution therefore *permits* eddies in the Arctic region at best. Over the broad Arctic Ocean shelf seas, the Rossby radius will be even smaller, and here such ocean general circulation models (OGCMs) are not even eddy-permitting. It follows that a key weakness of nearly all global ocean models used to study climate is the absence of an explicit representation of ocean mesoscale eddies, since their spatial scale is smaller than the scale typically resolved by model horizontal grid meshes.

These considerations motivate the push toward fully *mesoscale-eddy* ocean models, where the full dynamics and life cycle of baroclinic eddies is realistically represented over the entire global domain. Thanks to progress in ocean modeling and the advances in super-computing technology over the last decade, mesoscale-eddy numerical simulations are now a realistic choice to bring new insights into the physical processes operating in the ocean and to find application in Earth system modeling and forecasting [2].

In this context, CMCC has taken charge of developing a global ocean/sea ice configuration, hereunder called GLOB16, with a horizontal grid spacing ranging from about 6.9km at the equator to few kilometers



at high latitudes. It is so far the highest horizontal resolution implemented with the state-of-the-art modeling framework NEMO (Nucleus for European Modelling of the Ocean, <http://www.nemo-ocean.eu/>) at global scale. The numerical model is a coupled ocean/sea ice model, including a three-dimensional, free surface, hydrostatic, primitive-equation ocean general circulation model and a dynamic-thermodynamic sea-ice model.

The primary purpose of this report is to present the GLOB16 configuration, describe the general characteristics of the first simulation and give a brief overview of the obtained results. The report is organized as follows. Section 2 describes the numerical code and its parameterizations. Section 3 outlines the boundary conditions at the air-sea interface. Section 4 is dedicated to the model configuration and gives some technical details of the production of the run. Next, section 5 presents the post-processing method used to rebuild the output files. The last section gives some elements on the numerical results of the 10 year simulation to highlight the benefits of having such a high resolution.

2. THE NUMERICAL CODE

The high-resolution global simulation described here is performed using the NEMO model system. NEMO is a pan-European community ocean modelling framework owned and maintained by a consortium of institutes to which CMCC belongs.

The ocean general circulation model NEMO-OPA (Océan Parallélisé) is a finite difference, hydrostatic, primitive equation ocean general circulation model, with a free sea surface and a non-linear equation of state in the Jackett and McDougall formulation [22]. OPA describes the distribution of variables in a three-dimensional Arakawa-C-type grid centered at tracer points.

Prognostic variables (directly solved by the model equations) are the potential temperature, the salinity, the sea surface height and the 3D velocity field.

The physical framework used is version 3.4 of NEMO, whose complete description is provided by Madec et al. 2012 [30]. The revision number of the code used for this simulation is 4510. In addition, we apply some modifications to the base code. In particular, we modified the North Pole folding condition. Since release 3.4 of NEMO, the north fold horizontal boundary condition can be treated avoiding costly `mpi_gather` operations using an alternative method, which only performs direct "peer to peer" communications between each processor and its adjacent neighbours across the fold line. In our version of the code, a more recent optimization of the north-fold algorithm by Epicoco et al (2014) [10] has been added, which leads to an extra increase in model performances (up to 20% time-reduction on the used architecture). This new algorithm is activated setting `ln.nnogather = true` in the section "Massively Parallel Processing" (`nammpp`) of the ocean `namelist`, it avoids redundant operations and lets the parallel time to be inversely proportional with the number of processes. This optimization of the north fold condition is now used as standard for all CMCC global runs, and will be officially released in version 3.6 of NEMO.

In our version, the ocean component is coupled to the Louvain-la-Neuve sea Ice Model (LIM2) [11, 17]. LIM2 includes the representation of both the thermodynamic and dynamic processes. The ice dynamics are calculated according to external forcing from wind stress, ocean stress and sea-surface tilt and internal ice stresses using C-grid formulation [6]. The elastic viscous-plastic (EVP) formulation of ice dynamics by [19] is used. A comprehensive description of the sea-ice model used in GLOB16 is given in [21].



The C Pre-Processor (CPP) keys used in the compilations are listed in table 1.

Table 1. List of CPP keys

| | |
|------------------------|---|
| key_GLOB16: | GLOB16 horizontal grid with 98 vertical levels |
| key_trabbl: | bottom boundary layer parameterization for tracers |
| key_traldf_c2d: | 2D-varying coefficient for tracer lateral diffusion |
| key_dynldf_c2d: | 2D-varying coefficient for momentum lateral diffusion |
| key_dynspg_ts: | split-explicit free surface |
| key_zdftke: | TKE closure scheme for vertical mixing |
| key_lim2: | LIM2 sea ice model (with EVP rheology as default) |
| key_mpp_mpi: | massively parallel processing using MPI communications protocol |

OCEAN PHYSICS

The model uses a vector form momentum advection scheme (`ln_dynvor_een = .true.` in namelist section `namdyn_adv` on formulation of the momentum advection) with energy and enstrophy conserving conditions (`ln_dynvor_een = .true.` in `namdyn_vor`). The horizontal viscosity is bilaplacian with a value of $0.5e^9 m^4/s$ at the equator, reducing poleward as the cube of the maximum grid cell size. Tracer advection uses a total variance dissipation (TVD) scheme (`ln_traadv_tvd = .true.`). Lateral tracer mixing is performed with a geopotential biharmonic operator, the maximum value at the equator is $0.5e^9 m^4/s$. Relevant namelist parameters for horizontal physics are presented in table 2. Vertical mixing of tracers and momentum is parameterized using a modified version of

the turbulent kinetic energy (TKE) scheme by Gaspar et al. (1990) [15], embedded in NEMO by Blanke and Delecluse (1993) [5] (see Madec et al. (1998) [29] for details). The turbulent length scale calculation allows the length scale to be limited not only by the distance to the surface or to the ocean bottom but also by the distance to a strongly stratified portion of the water column such as the thermocline (`nn_mxl = 3`). Unresolved vertical mixing processes are represented by a background vertical eddy diffusivity of $1.2e^{-5} m^2/s$ and a background vertical eddy viscosity of $1.2e^{-4} m^2/s$. The depth of TKE penetration below the mixed layer increases from 0.5m at the equator to 30m poleward of 40° (`nn_htau = 1`). Vertical density instabilities are treated with enhanced vertical diffusivity (`evd`) at the interface of two layers with density inversion (`ln.zdfevd = true`). The vertical eddy coefficients on both momentum and tracers (`nn_evdn = 1`) are assigned to be larger where the stratification is unstable, with the `evd` mixing coefficient set to the default $10m^2/s$. The TKE turbulent closure model does not apply any specific modification in ice-covered regions. Relevant namelist data for vertical physics are presented in table 3. Bottom boundary layer (bbl) parameterization is used for tracers, which allows a direct communication between two adjacent bottom cells at different levels, whenever the densest water is located above less dense water. Only bbl enhanced diffusion (not advection) is applied (lateral mixing coefficient `rn_ahtbbl = m^2/s`). The simulation is performed with free-slip lateral boundary condition (`rn_shlat = 0`). In this first GLOB16 simulation, the lateral boundary conditions are not locally modified to no-slip or partial slip in any specific areas. A classical quadratic bottom friction is used, with a drag coefficient of `rn_bfri2 = 1e^{-3} m^2/s^2` without specific amplification in straits.

**Table 2. Horizontal physics**

```
!-----
&namdyn_ldf ! lateral diffusion on momentum
!-----
!
!           ! Type of the operator :
ln_dynldf_lap = .false. ! laplacian operator
ln_dynldf_bilap = .true. ! bilaplacian operator
!
!           ! Direction of action :
ln_dynldf_level = .false. ! iso-level
ln_dynldf_hor = .true. ! horizontal (geopotential) (require "key_ldfslp" in s-coord.)
ln_dynldf_iso = .false. ! iso-neutral (require "key_ldfslp")
!
!           ! Coefficient
rn_ahm_0_lap = 1.e2 ! horizontal laplacian eddy viscosity [m2/s]
rn_ahmb_0 = 0. ! background eddy viscosity for ldf_iso [m2/s]
rn_ahm_0_blp = -0.5e9 ! horizontal bilaplacian eddy viscosity [m4/s]
!-----
&namtra_ldf ! lateral diffusion scheme for tracer
!-----
!
!           ! Type of the operator :
ln_traldf_lap = .false. ! laplacian operator
ln_traldf_bilap = .true. ! bilaplacian operator
!
!           ! Direction of action :
ln_traldf_level = .false. ! iso-level
ln_traldf_hor = .true. ! horizontal (geopotential) (require "key_ldfslp" when ln_sco=T)
ln_traldf_iso = .false. ! iso-neutral (require "key_ldfslp")
ln_traldf_grif = .false. ! griffies skew flux formulation (require "key_ldfslp")
ln_traldf_gdia = .false. ! griffies operator strfn diagnostics (require "key_ldfslp")
ln_triad_iso = .false. ! griffies operator calculates triads twice => pure lateral mixing in ML
ln_botmix_grif = .false. ! griffies operator with lateral mixing on bottom (require "key_ldfslp")
!
!           ! Coefficient
rn_aht_0 = -0.5e9 ! horizontal eddy diffusivity for tracers [m2/s]
rn_ahtb_0 = 0. ! background eddy diffusivity for ldf_iso [m2/s]
rn_aeiv_0 = 1.e1 ! eddy induced velocity coefficient [m2/s] (require "key_traldf_eiv")
```



Table 3. Vertical physics

```

!-----
&namzdf ! vertical physics
!-----
rn_avm0   = 1.2e-4 ! vertical eddy viscosity [m2/s] (background Kz if not "key_zdfcst")
rn_avt0   = 1.2e-5 ! vertical eddy diffusivity [m2/s] (background Kz if not "key_zdfcst")
nn_avb    = 0      ! profile for background avt & avm (=1) or not (=0)
nn_havtb  = 0      ! horizontal shape for avtb (=1) or not (=0)
ln_zdfevd = .true.  ! enhanced vertical diffusion (evd) (T) or not (F)
nn_evdm   = 1      ! evd apply on tracer (=0) or on tracer and momentum (=1)
rn_avevd  = 10.    ! evd mixing coefficient [m2/s]
ln_zdfnpc = .false. ! Non-Penetrative Convective algorithm (T) or not (F)
nn_npc    = 1      ! frequency of application of npc
nn_npcp   = 365    ! npc control print frequency
ln_zdfexp = .false. ! time-stepping: split-explicit (T) or implicit (F) time stepping
nn_zdfexp = 3      ! number of sub-timestep for ln_zdfexp=T

!-----
&namzdf_tke ! turbulent eddy kinetic dependent vertical diffusion ("key_zdf_tke")
!-----
rn_ediff  = 0.1    ! coef. for vertical eddy coef. (avt=rn_ediff*mxl*sqrt(e) )
rn_ediss  = 0.7    ! coef. of the Kolmogoroff dissipation
rn_ebb    = 60     ! coef. of the surface input of tke (=67.83 suggested when ln_mxl0=T)
rn_emin   = 1.e-6  ! minimum value of tke [m2/s2]
rn_emin0  = 1.e-4  ! surface minimum value of tke [m2/s2]
nn_mxl    = 3      ! mixing length: = 0 bounded by the distance to surface and bottom
              ! = 1 bounded by the local vertical scale factor
              ! = 2 first vertical derivative of mixing length bounded by 1
              ! = 3 as =2 with distinct dissipative an mixing length scale
nn_pdl    = 1      ! Prandtl number function of Richardson number (=1,avt=pdl(Ri)*avm) or not (=0)
ln_mxl0   = .true. ! surface mixing length scale = F(wind stress) (T) or not (F)
rn_mxl0   = 0.01   ! surface buoyancy length scale minimum value
ln_lc     = .true. ! Langmuir cell parameterisation (Axell 2002)
rn_lc     = 0.15   ! coef. associated to Langmuir cells
nn_etau   = 1      ! penetration of tke below the mixed layer (ML) due to internal & inertial waves
              ! = 0 no penetration
              ! = 1 add a tke source below the ML
              ! = 2 add a tke source just at the base of the ML
              ! = 3 as = 1 applied on HF part of the stress ("key_coupled")
rn_efr    = 0.05   ! fraction of surface tke value which penetrates below the ML (nn_etau=1 or 2)
nn_htau   = 1      ! type of exponential decrease of tke penetration below the ML
              ! = 0 constant 10 m length scale
              ! = 1 0.5m at the equator to 30m poleward of 40 degrees

```



3. SURFACE BOUNDARY CONDITION

The surface boundary conditions are prescribed to the model using the CORE bulk formulation [24] (with `ln_blk_core` set `.true.`) and computed using bulk formulae, atmospheric fields and ocean/sea ice variables. CORE bulk formulae need 8 different atmospheric fields as input:

- Turbulent variables: 2m air temperature (`t2m`), 2m specific humidity (`q2m`), 10m 10m wind velocity components (`u10m` and `v10m`).
- Fresh water fluxes: total precipitation (`precip`) and solid precipitation (`snow`).
- Radiative fluxes: short-wave (solar) radiative flux (`swrd`), long-wave (thermal) radiative flux (`lwrd`).

These formulae compute (in the `sbcblk_core.F90` routine) sensible and latent heat fluxes along with evaporation and wind stresses (calculated as a function of the difference between 10m wind components and the ocean surface velocity). Solar and non-solar radiative fluxes and total and solid precipitations are processed so as to supply complete surface boundary conditions to the ocean and sea ice models. Forcing fields are provided from ERA-Interim global atmospheric reanalysis [9], released by European Centre for Medium-Range Weather Forecasts (ECMWF), with $0.75^\circ \times 0.75^\circ$ spatial resolution (T255 Gaussian grid). The turbulent variables are 3-hourly and radiative and freshwater fluxes are daily. CORE bulk formulations, designed to handle the CORE forcing (based on NCEP reanalysis and satellite data) do not require modifications when applying ERA-Interim fields.

The forcing routine and the ice model are called only every 4 time steps (`nn_fsbc` = 4).

With a time step of 200sec, they are called every ~ 13 mins, about 110 times in a day, which is reasonable compared to the highest frequency of the forcing variables (3 hrs).

Due to the high vertical resolution near the surface, diurnal cycle is imposed on solar flux (`ln_dm2dc` = `.true.`). The daily averaged short wave flux is spread over the day according to time and geographical position [4]. This parameterization yields a better representation of the night-time convection, which takes place in the 5m upper layer. The mean sea level is free to drift (`nn_fwb` = 0). See table 4 for details. The trend associated with the penetration of the solar radiation is added to the temperature trend. Shortwave penetration is applied (`ln_traqsr` = `.true.`) through the RGB (Red-Green-Blue) formulation (`ln_qsr_rgb` = `.true.`) that splits the visible light into three wavebands. This model reproduces closely the light penetration profiles predicted by a full spectral model, but with greater computational efficiency [25]. The penetration is modulated by a constant chlorophyll value (`nn_chdta` = 0). All surface forcing fields are interpolated *on the fly* providing an interpolation weights file, instead of pre-processing them.

RUNOFF

A monthly climatology of coastal and river runoff is used (`ln_rnf` = `.true.`) and read from file. The field is inferred from Dai and Trenberth dataset [7], which uses 99 major rivers and coastal runoff estimates, with a global annual discharge of ~ 1.32 Sv. The input file, available for a $1/4^\circ$ configuration, was interpolated offline on the GLOB16 grid. No special treatment is applied at rivers mouths. The fresh water is added to the surface box only, assumed to be fresh (0 psu) and at sea surface temperature.



Table 4. Surface boundary condition

```

!-----
&namsbc ! Surface Boundary Condition (surface module)
!-----
nn_fsbc      = 4    ! frequency of surface boundary condition computation
                ! (also = the frequency of sea-ice model call)
ln_ana       = .false. ! analytical formulation (T => fill namsbc_ana )
ln_flux      = .false. ! flux formulation (T => fill namsbc_flux )
ln_blk_clio  = .false. ! CLIO bulk formulation (T => fill namsbc_clio)
ln_blk_core  = .true.  ! CORE bulk formulation (T => fill namsbc_core)
ln_blk_mfs   = .false. ! MFS bulk formulation (T => fill namsbc_mfs )
ln_cpl       = .false. ! Coupled formulation (T => fill namsbc_cpl )
ln_apr_dyn   = .false. ! Patm gradient added in ocean & ice Eqs. (T => fill namsbc_apr )
nn_ice       = 2    ! =0 no ice boundary condition ,
                ! =1 use observed ice-cover ,
                ! =2 ice-model used ("key_lim3" or "key_lim2")
ln_dm2dc     = .true.  ! daily mean to diurnal cycle on short wave
ln_rnf       = .true.  ! runoffs (T => fill namsbc_rnf)
ln_ssr       = .true.  ! Sea Surface Restoring on T and/or S (T => fill namsbc_ssr)
nn_fwbc     = 0    ! FreshWater Budget: =0 unchecked
                ! =1 global mean of e-p-r set to zero at each time step
                ! =2 annual global mean of e-p-r set to zero
                ! =3 global emp set to zero and spread out over erp area
ln_cdgw      = .false. ! Neutral drag coefficient read from wave model (T => fill namsbc_wave)

!-----
&namsbc_core ! namsbc_core CORE bulk formulae
!-----
!      ! file name ! frequency (hours) ! variable ! time interp. ! clim ! 'yearly' ! weights ! rotation !
!      ! (if <0 months) ! name ! (logical) ! (T/F) ! 'monthly' ! filename ! pairing !
sn_wndi = 'ERA-INT_u10m' , 3 , 'u10m' , .true. , .false. , 'yearly' , 'weights_bicubic' ,
                'Uwnd'
sn_wndj = 'ERA-INT_v10m' , 3 , 'v10m' , .true. , .false. , 'yearly' , 'weights_bicubic' ,
                'Vwnd'
sn_qsr = 'ERA-INT_swrd' , 24 , 'swrd' , .true. , .false. , 'yearly' , 'weights_bicubic' ,
sn_qlw = 'ERA-INT_lwrd' , 24 , 'lwrd' , .true. , .false. , 'yearly' , 'weights_bicubic' ,
sn_tair = 'ERA-INT_t2m' , 3 , 't2m' , .true. , .false. , 'yearly' , 'weights_bicubic' ,
sn_humi = 'ERA-INT_q2m' , 3 , 'q2m' , .true. , .false. , 'yearly' , 'weights_bicubic' ,
sn_prec = 'ERA-INT_precip' , 24 , 'precip' , .true. , .false. , 'yearly' , 'weights_bicubic' ,
sn_snow = 'ERA-INT_snow' , 24 , 'snow' , .true. , .false. , 'yearly' , 'weights_bicubic' ,
sn_tdif = 'qscat_corr' , -1 , 'tauint' , .true. , .false. , 'yearly' , " , "

ln_2m      = .true. !sd .true. ! air temperature and humidity referenced at 2m (T) instead 10m (F)
ln_taudif  = .false. ! HF tau contribution: use "mean of stress module - module of the mean stress" data
rn_pfac    = 1.    ! multiplicative factor for precipitation (total & snow)

```



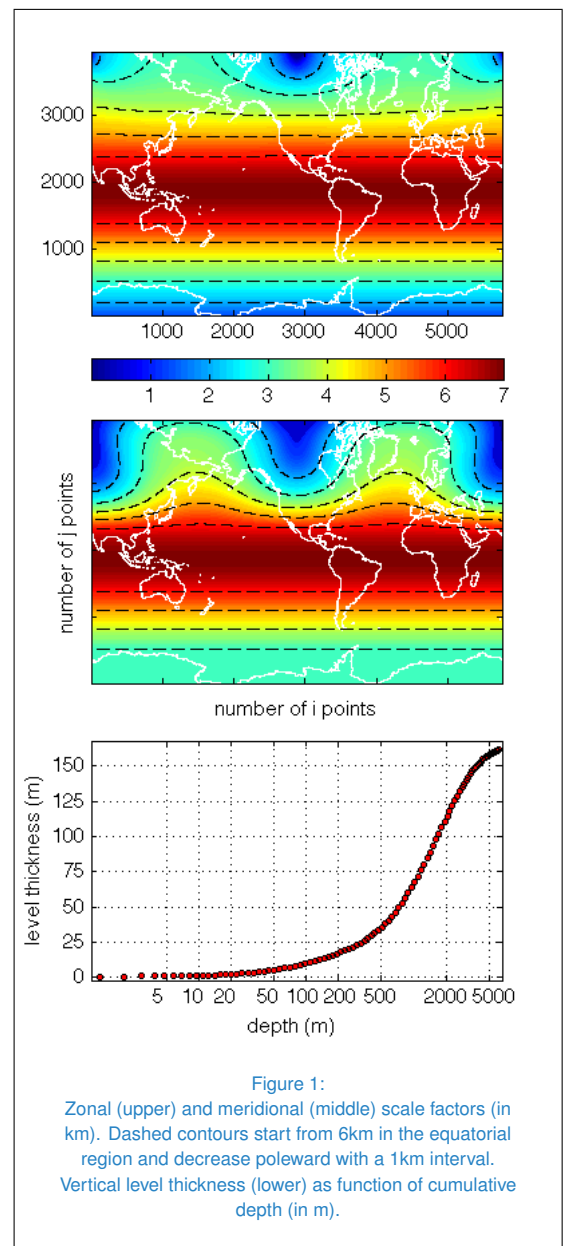
SURFACE RESTORING

Sea surface restoring to both observed sea surface temperature (SST) and salinity (SSS) is used (`ln_ssr = .true.`, `nn_sstr = 1` and `nn_ssr = 2`). SST is restored towards the NOAA Optimum Interpolation $1/4^\circ$ Daily Sea Surface Temperature Analysis [35] with a constant damping term of $200 \text{ W/m}^2/\text{K}$ that corresponds to a restoring time of 12 days. A damping term is added to the surface freshwater flux to avoid drifts of the model salinity and an effect on the overturning circulation. We used standard SSS restoring toward the monthly objective analyses from the EN4 data set of the Met Office Hadley Centre [16]. The piston velocity used for the SSS restoring (`rn_deds`) is set to $\sim 167 \text{ mm/day}$ that corresponds to a time scale of 60 days for the upper 10 meters of the ocean. The restoring is identical for the open sea and ice covered areas. No relaxation has been applied to 3D tracer, nowhere in the ocean. The namelist section related to the sea surface restoring is presented in table 5.

4. MODEL CONFIGURATION GRID

GLOB16 makes use of a non-uniform tri-polar grid with a T-point pivot for the north fold condition, developed at CMCC. The grid has a $1/16^\circ$ horizontal resolution that corresponds to 6.9km at the equator and increases poleward (the grid size is scaled by the cosine of the latitude, except in polar areas, e.g. $\sim 5.5 \text{ km}$ at 40° , $\sim 4 \text{ km}$ at 60°), leading to horizontal dimensions of 5762×3963 grid points. Zonal and meridional scale factors are represented in Figure 1. This grid consists of a Mercator grid from 60°S to 20°N , and a non-geographic quasi-isotropic grid north of it. The location of the geographical South Pole is conserved and the domain extends southwards to 78°S to include the ice shelf edge in the Weddell and Ross

Seas. Meridional scale factor is maintained constant at 3km south of 60°S . To avoid singularities associated with the convergence of meridians at the North Pole, two distinct poles are introduced in northern hemisphere, positioned over land in Canada (109°W , 62°N) and in Siberia (71°E , 53°N). Locations of the singularities of the northern grid are such that the





minimum horizontal resolution is ~ 2 km around Victoria Island. Ocean and sea-ice are on the same horizontal grid.

The vertical coordinate system is based on fixed geopotential levels ("z-levels"). We consider the needs of vertical resolution in concert with the refinements of horizontal spacing in order to accurately capture the enhanced vertical motions and structure within eddy features. The vertical grid consists of 98 vertical levels with a grid spacing increasing from approximately 1m near the surface to 160m in the deep ocean (Fig. 1).

BATHYMETRY

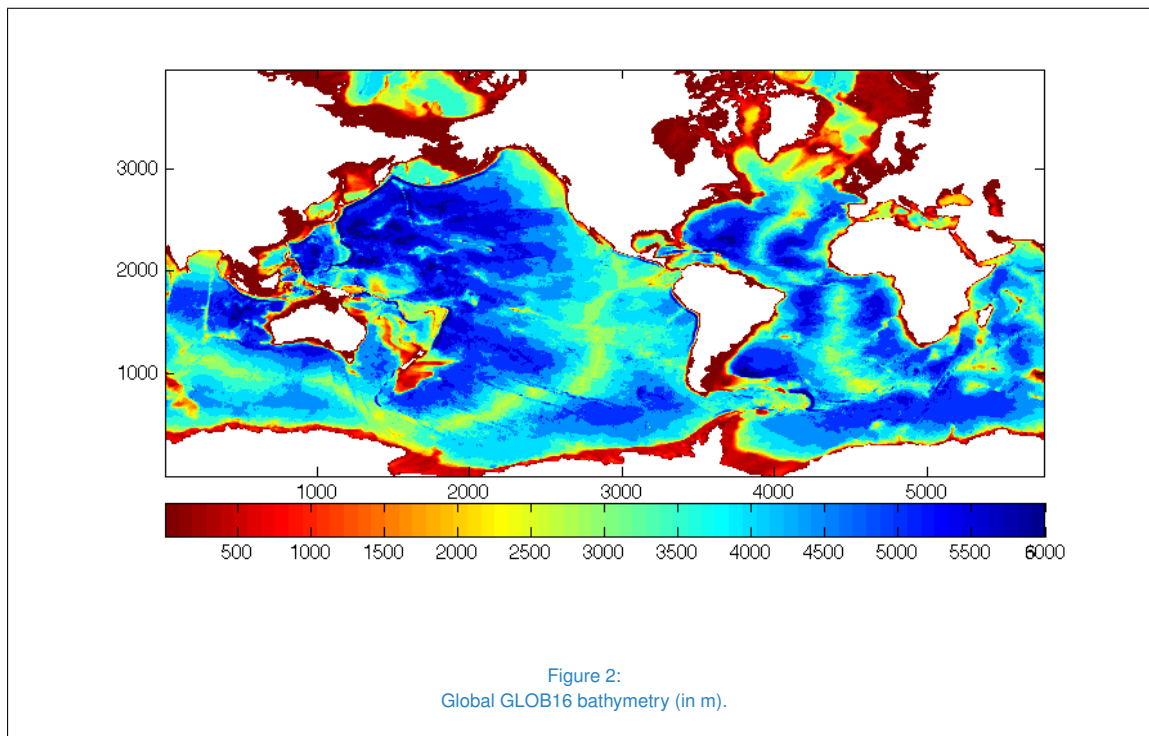
The GLOB16 bathymetry, presented in Figure 2, is derived from three separate topographic products:

- the 2-minute Etopo2 bathymetry of the National Geophysical Data Center (NGDC) [32], which is a combination of

the satellite-based bathymetry by Smith and Sandwel [37] and the International Bathymetric Chart of the Arctic Ocean (IBCAO) [23], is used for the deep ocean (below 300m).

- the 1-minute GEBCO (General Bathymetric Chart of the Oceans) [20] is used on shelf areas shallower than 200m.
- Bedmap2 [12] is used for the Antarctic region, south of 60° S.

GEBCO and Etopo2 are combined with a linear damping between 200m and 300m. The resulting product is connected to BEDMAP2 in the southernmost ocean via a sponge layer covering 10 grid rows. The interpolation onto the model grid is conducted by taking all the original grid points falling into a GLOB16 grid box, and taking the median of those points. The topography has been smoothed by two passes of a uniform shapiro filter with weight





($w=0.6$). Hand-editing is performed in key areas, as channels and small islands that may have been smoothed out by the interpolation process, e.g. the Indonesian and Canadian archipelagos. The Caspian Sea is all derived from Etopo2, areas shallower than 20m are discharged to clearly mark the northern boundary. The Black Sea is connected to the Marmara Sea through a channel that mimics the Bosphorus Strait (1 grid point wide). Detailed list of all modifications of model bathymetry is available upon request to authors. The minimum depth in the model is set to 10m. The maximum depth allowed in the model is 6000m. To induce a better representation of steep topographic gradients and deep oceanic circulation [3], partial cell representation of the topography is allowed at the sea floor, i.e. the depth of the bottom cell is variable and adjustable to the real depth of the ocean. To calculate the partial cell layer thickness rn_e3zps_min is set to 25 and rn_e3zps_rat to 0.5. Section "space and time domain" (namdom) of the namelist is presented in table 6.

INITIAL CONDITIONS

The simulations started from rest in 2003, with initial climatological temperature and salinity derived from the World Ocean Atlas 2013 set of climatologies [28, 39]. The 1995-2004 decade is used to represent year 2003. The 3D temperature and salinity are a combination of monthly climatologies (covering the upper ~ 1500 m) and seasonal climatologies for the deeper ocean, with a maximum of 102 vertical levels. Both products, with an original $1/4^\circ$ horizontal resolution, were re-gridded on GLOB16 3D grid.

The initial conditions for the sea ice (ice concentration, ice thickness) are taken from a CMCC ocean reanalysis [38], run at $1/4^\circ$ horizontal resolution, forced by ERA-Interim atmospheric reanalysis, and then interpolated on the GLOB16 grid. This initial condition corresponds

to mean January 2003.

RUNNING STRATEGY

The run started 1st January 2003 and ended 31st December 2013. The time step used at the beginning of the simulation was 20sec for the first 3 days, and then increased progressively to 50sec for days 4-31, 100sec for days 32-59 and 200sec after.

The run was performed on iDataPlex architecture, based on Intel Sandy Bridge processors, located at Barcelona Supercomputing Center in Spain (within the framework of the ENS4OCEAN project awarded in the PRACE 8th Regular Call). The simulation used 4080 CPU cores. The domain decomposition used is 87 x 66 cores along x- and y- directions respectively (land domain were eliminated). Each core computes 66 x 62 grid points. We reach computing performance of 112000 CPU hours per simulated year (wall-clock time ~ 13 hrs).

Model output is done as 5-days averages. The 2D and 3D model output approaches 3Tb per year (plus ~ 2.3 Tb for restart files). Monthly and annual means are computed in the post processing. We also computed climatologies over the periods 2004-2013.

Ten simulation years is sufficient time for the model to reach a quasi-equilibrium state, where the velocity field has adjusted to the initial density field. This simulation is therefore appropriate for studying the dynamics of the ocean circulation on time scales of a decade or less, but it is not appropriate for studying the long-term evolution of deep-water masses or climate variability on longer time scales.

5. IMPLEMENTATION OF OPTIMIZED COLLECTIVE IO FOR VARIABLE RECONSTRUCTION

The postprocessing mainly consists in the rebuild of the 2D and 3D model output over the



Table 5. Sea Surface Restoring

```

!-----
&namcbc_ssr ! surface boundary condition : sea surface restoring
!-----
!      ! file name ! frequency (hours) ! variable ! time interp. ! clim ! 'yearly' ! weights ! rotation !
!!      ! (if <0 months) ! name ! (logical) ! (T/F) ! 'monthly' ! filename ! pairing !
sn_sst = 'sst',          24,          'sst',          .true. ,   .false. , 'daily', 'weights_bicubic', "
sn_sss = 'sss_data',    -1,          'salinity',    .true. ,   .false. , 'yearly', 'weights_bicubic', "

cn_dir_sst   = '/gpfs/projects/pr1e7600/ORCA16/NOAA_SST/sst_data/'
cn_dir_sss   = '/gpfs/projects/pr1e7600/ORCA16/EN4_OA/sss_data/'
nn_sstr      =      1      ! add a retroaction term in the surface heat flux (=1) or not (=0)
nn_ssr       =      2      ! add a damping term in the surface freshwater flux (=2)
              ! or to SSS only (=1) or no damping term (=0)
rn_dqdt      =   -200.    ! magnitude of the retroaction on temperature [W/m2/K]
rn_deds      =  -166.67  ! magnitude of the damping on salinity [mm/day]
ln_ssr_bnd   =   .false.  ! flag to bound erp term (associated with nn_ssr=2)
rn_ssr_bnd   =      0.    ! ABS(Max/Min) value of the damping erp term [mm/day]
    
```

Table 6. Space and time domain

```

!-----
&namdom ! space and time domain (bathymetry, mesh, timestep)
!-----
nn_bathy     =      1      ! compute (=0) or read (=1) the bathymetry file
nn_closea   =      1      ! remove (=0) or keep (=1) closed seas and lakes (ORCA)
nn_msh       =      0      ! create (=1) a mesh file or not (=0)
rn_hmin      =    10.     ! min depth of the ocean (>0) or min number of ocean level (<0)
rn_e3zps_min =    25.     ! partial step thickness is set larger than the minimum of
rn_e3zps_rat =    0.5     ! rn_e3zps_min and rn_e3zps_rat*e3t, with 0<rn_e3zps_rat<1
!
rn_rdt       =   _TS_    ! time step for the dynamics (and tracer if nn_acc=0)
nn_baro      =    120     ! number of barotropic time step ("key_dynspg_ts")
rn_atfp      =     0.1    ! asselin time filter parameter
nn_acc       =      0     ! acceleration of convergence : =1 used, rdt < rdtra(k)
              ! =0, not used, rdt = rdtra
rn_rdtmin    =   _TS_    ! minimum time step on tracers (used if nn_acc=1)
rn_rdtmax    =   _TS_    ! maximum time step on tracers (used if nn_acc=1)
rn_rdth      =     10.    ! depth variation of tracer time step (used if nn_acc=1)
    
```



global grid. As the model was run using 4080 CPUs, the output is split in 4080 files, each containing the field values referring to a x - y partition of the global domain. The rebuild algorithm available in NEMO is not able to manage such a large number of NetCDF files to reconstruct global variables at these horizontal and vertical resolutions.

Standard IO routines have been designed for efficiently managing datasets that satisfy some size requirements [1]. New prescriptions on file format and some improvements on serial IO are therefore needed to relax these size restrictions, allowing high-resolution simulations to be properly stored and analysed.

Concerning the file format, state-of-the-art simulations show very thick meshes that cannot be indexed or stored with softwares based on 32-bit pointers:

$$\underbrace{\dim(x) \times \dim(y) \times \dim(z)}_{\simeq 2.23 * 10^9} > \underbrace{\dim(32\text{-bit pointer})}_{2^{31} - 1 \simeq 2.14 * 10^9},$$

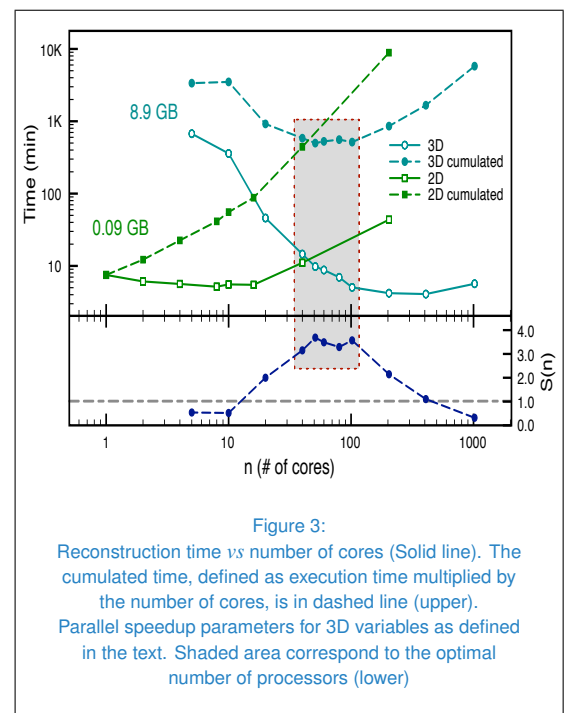
meaning that the number of grid points exceeds the size of a classic NetCDF variable. Newer versions¹ adopt 64-bit pointers but they are not backward compatible with earlier releases, thus limiting their portability. To save the latter we kept the classic NetCDF version by exploiting Large File Support (LFS). Thanks to LFS, each dataset can correctly manage one single variable exceeding the size limit.

At current resolution, any NEMO output is spread over more than 4000 datasets that must be merged back before further manipulation. A massive use of IO routines is therefore needed. Standard IO allows only serial access: ideally all data should be shipped to a single process slowing down the overall execution in the best case. Adding OpenMP/MPI environment on top of NetCDF, is of little help for reconstruction purpose since each concurrent process can use only serial IO.

We implement a high-performance collective

IO routines based on parallel NetCDF package (pNetCDF) [26]. pNetCDF is an independent release from Argonne Laboratory with integrated parallel IO specifically designed for this kind of datasets [26, 27]. Original API features are mostly preserved and a new MPI communicator is added to point processes devoted to IO.

This package seems to perform better than NetCDF-4 with collective IO from HDF5 library [14].



Variable reconstruction performances with pNetCDF have been optimized and tested on *Marenostrum III* cluster in Barcelona Supercomputing Centre (BSC). Collective IO have a great impact on 3D variables while shows little effects on 2D ones (Fig. 3). For large files, the execution time sharply reduces by increasing the number of processes from 13 hours to a bunch of minutes. The overall cumulated time decreases accordingly, meaning that we are actually saving time and power on the clus-

¹from NetCDF-3.6 in 64-bit offset mode



ter increasing the number of cores employed. This trend is far from being common, parallel speedup is super-linear in this range.

A rough estimate of IO performance for large variables is shown in lower panel of Figure 3. We compare these trends versus a virtual OpenMP algorithm limited to a single node (16 cores). The parallel speed up parameter $S(n)$ is now the ratio between cumulated time of MP and MPI process [33] :

$$S(n) = \frac{T_{MP}(1 \text{ node})}{T_{MPI}(n)} \quad (1)$$

As can be clearly seen we gain a factor 4 in the optimal range (shaded window). The trend reverts with more than 100 cores when intra-communications among processes become important.

6. RESULTS

The main objective of this report is to describe the characteristics of the GLOB16 configura-

tion and present the first decadal simulation. Validation of the numerical results is out of the scope. Detailed analyses will follow in later manuscripts and we will rely on comparisons with other global runs, as well as with data, as a means of assessing the quality of this simulation. However, the basic performance of the OGCM is presented in this section through maps of the major ocean variables averaged over the last year of integration, 2013, and time-series of mass and heat fluxes at key-locations. First, annual mean over the last year of integration (2013) are shown for global SST (in Fig. 4) and SSS (in Fig. 5) and sea surface Height (in Fig. 6). The depth of the mixed layer is plotted, as monthly mean, for March in the northern hemisphere, for September in the southern one (in Fig. 7). Then, we proceed showing the barotropic stream function in the North Atlantic sector (in Fig. 8).

A remarkable feature of GLOB16, due to the

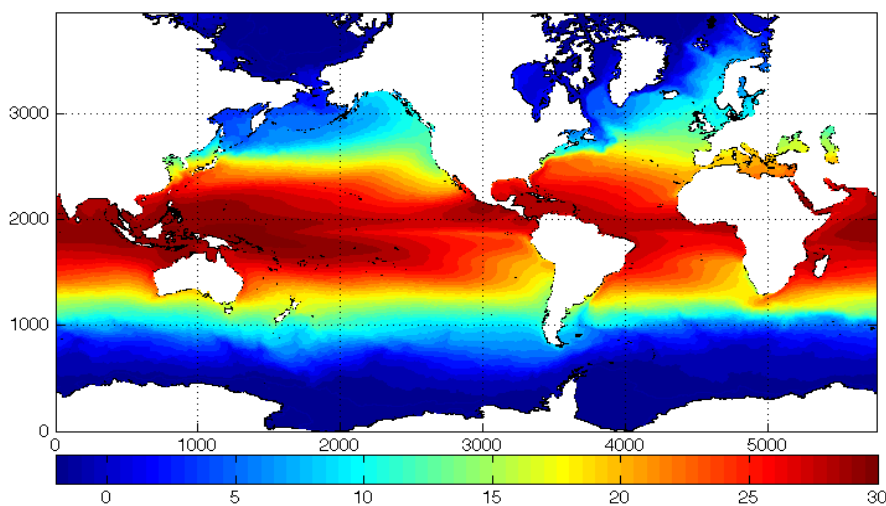
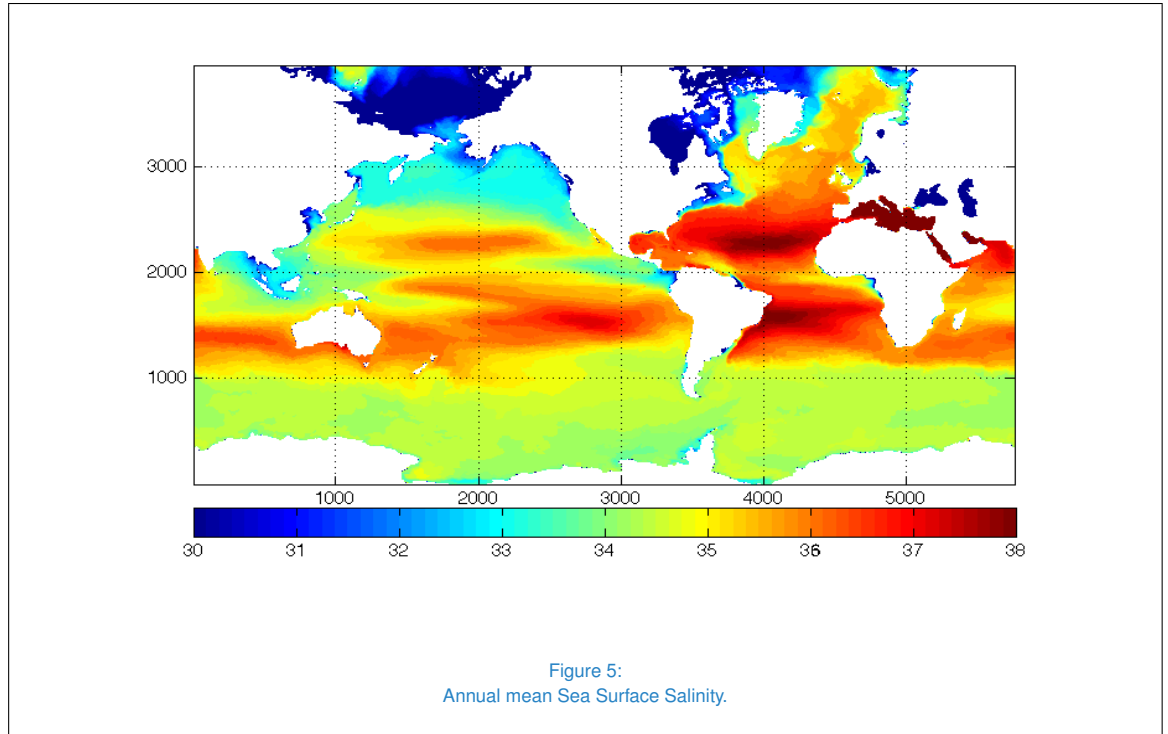


Figure 4:
Annual mean Sea Surface Temperature (in °C).



1/16° horizontal resolution, is the emergence of a ubiquitous mesoscale eddy field (see Fig. 9) that is substantially stronger than what is typically produced in global simulations at lower resolution. As expected, the simulation exhibits extremely turbulent behavior, with eddy energy agreeing well, by many measures, with satellite altimetry in both location and magnitude in most high-activity areas (not shown).

The general circulation is well represented (not shown), with acceptable values for overturning transports of mass and heat, and good agreement with transport estimates of the major current systems. As indicator of the strength of the global thermohaline circulation, we present the meridional overturning streamfunction, zonally averaged in the global domain and in the

North Atlantic Ocean (Fig. 10). The variations during the model integration of two important climatic indexes, the strength of the overturning streamfunction in the North Atlantic and the associated poleward heat fluxes at 26°N, are computed and compared with the RAPID arrays [13] in Figure 11. We conclude considering the transports of mass, through the whole water, across some key sections for the global circulation: the volume transports associated to inflows at the Bering Strait and the Barents Sea Opening, and to outflows at the Fram and Davis strait (Figs. 12), the outflow transports from the Nordic Sea into the North Atlantic ocean across Denmark Strait (Fig. 13), and the Antarctic Circumpolar Current (ACC) transport through the Drake Passage (Figs. 14).

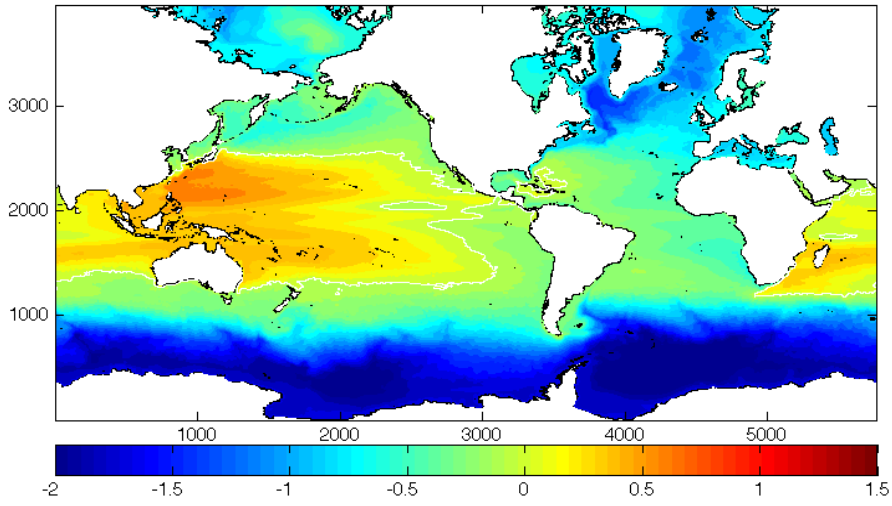


Figure 6:
Annual mean Sea Surface Height (in m). The white line indicates zero contour.

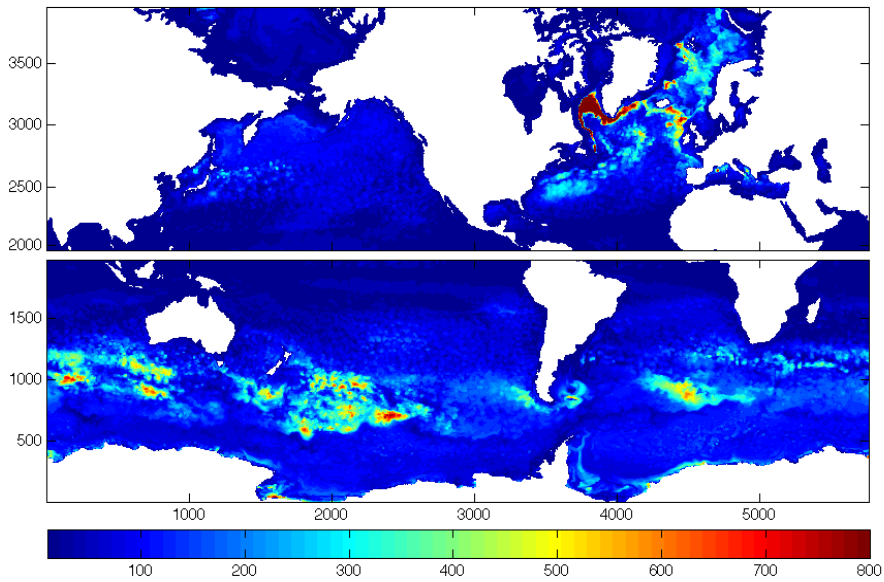


Figure 7:
Mixed layer depth averaged on March (September) 2013 for the northern (southern) hemisphere (in m).

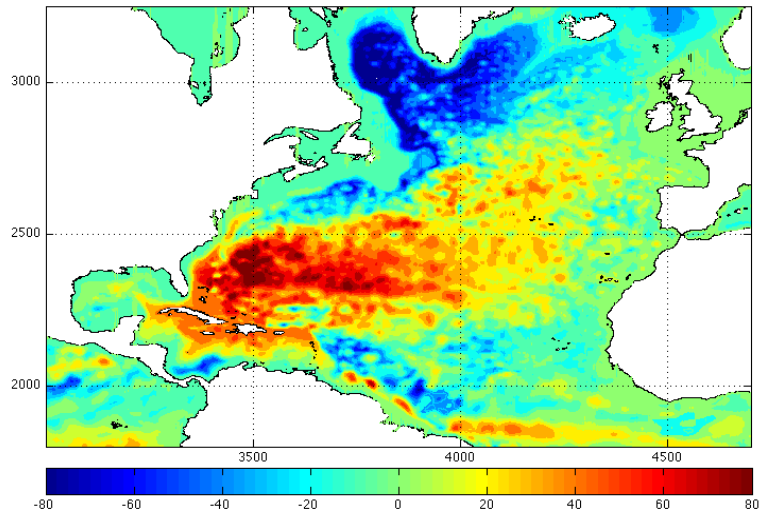


Figure 8:
Annual mean Barotropic Streamfunction in the North Atlantic Ocean (in Sv).

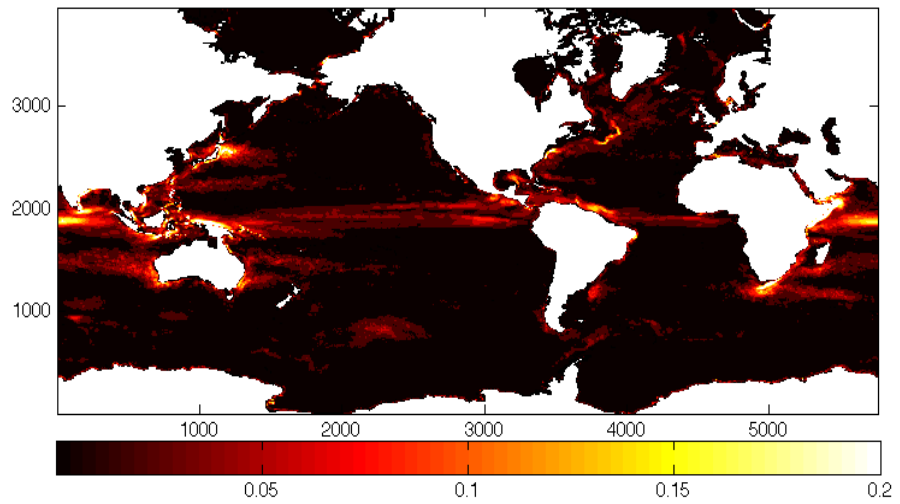


Figure 9:
Annual mean surface Eddy Kinetic Energy (in m^2/s^2).

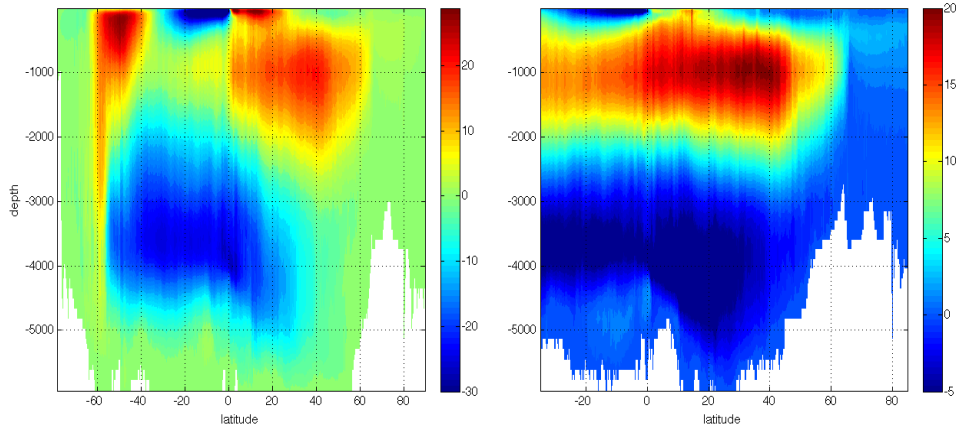


Figure 10:
Annual mean Meridional Overturning Circulation for the global (left) and the North Atlantic Ocean (right) (in Sv).

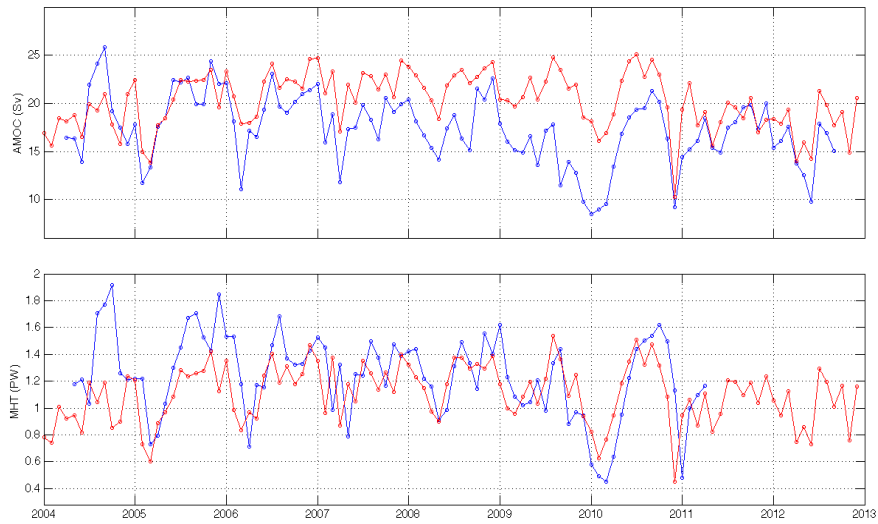


Figure 11:
Time-series of the maximum overturning (in Sv) and the heat transport (in PW) at 26°N in the Atlantic Ocean as numerically calculated (red lines) compared to RAPID data set (blue lines).

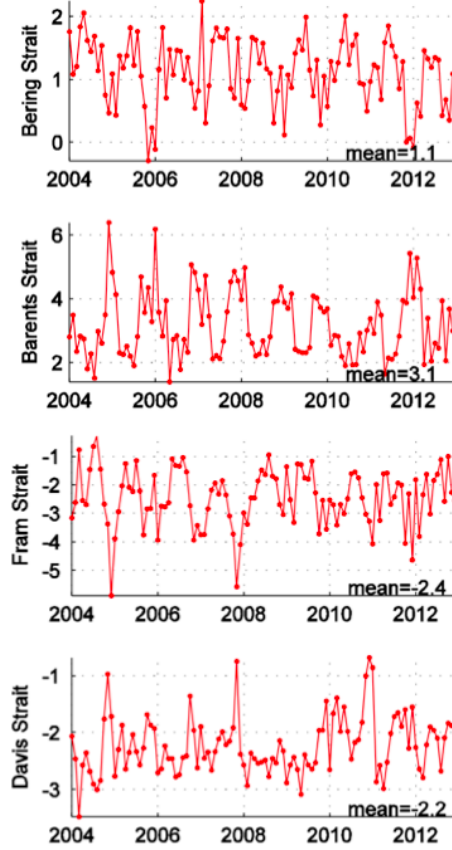


Figure 12:
Time-series of the volume transport (in Sv) across the Bering Strait, the Barents Sea Opening, the Fram and the Davis straits. Positive (negative) values correspond to northward (southward) flow.

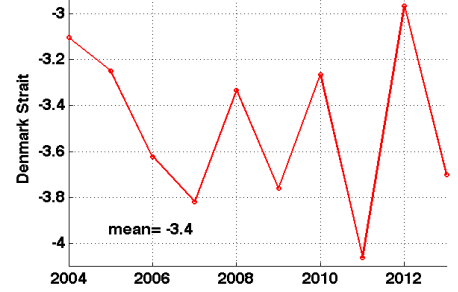


Figure 13:
Time-series of the volume transport (in Sv) across the Denmark Strait. Negative values indicate southward transport.

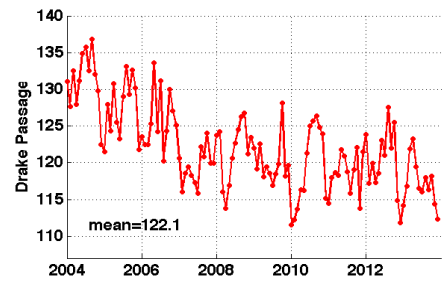


Figure 14:
Time-series of the volume transport (in Sv) through the Drake Passage.



Bibliography

- [1] Online netcdf users' guide. <http://www.unidata.ucar.edu/packages/-netcdf/docs/netcdf/Large-File-Support.html>.
- [2] *CLIVAR Exchanges No.65. Special Issue: High Resolution Ocean Climate Modelling. Vol.19, No.2.* The International CLIVAR Project Office ISSN No: 1026-0471, July 2014.
- [3] B. Barnier, G. Madec, T. Penduff, J.M. Molines, A.M. Treguier, J. Le Sommer, A. Beckmann, A. Biastoch, C. Boning, J. Dengg, C. Derval, E. Durand, S. Gulev, E. Remy, C. Talandier, S. Theetten, M. Maltrud, J. McClean, and B. De Cuevas. Impact of partial steps and momentum advection schemes in a global ocean circulation model at eddy-permitting resolution. *Ocean Dynamics*, 56:543–567, 006.
- [4] D. Bernie, E. Guilyardi, G. Madec, J. M. Slingo, and S. J. Woolnough. Impact of resolving the diurnal cycle in an ocean–atmosphere gcm. part 1: a diurnally forced ogcm. *Climate Dynamics*, 29(6):575–590, 2007.
- [5] B. Blanke and P. Delecluse. Low frequency variability of the tropical atlantic ocean simulated by a general circulation model with mixed layer physics. *Journal of Physical Oceanography*, 23:1363–1388, 1993.
- [6] S. Bouillon, M.M. Maqueda, V. Legat, and T. Fichefet. An elastic-viscousplastic sea ice model formulated on arakawa b and c grids. *Ocean Modelling*, 27:174–184, 2009.
- [7] R. Bourdalle-Badie and A.M. Treguier. A climatology of runoff for the global ocean-ice model ORCA025. Technical Report MOO-RP-425-365-MER, Mercator-Ocean report, 2006.
- [8] D. Chelton, R. DeSzoek, M. Schlax, K. El Naggar, and N. Siwertz. Geographical variability of the first baroclinic rossby radius of deformation. *Journal of Physical Oceanography*, 28:433–460, 1998.
- [9] D.P. Dee, S.M. Uppala, A.J. Simmons, P. Berrisford, P. Poli, S. Kobayashi, U. Andrae, M.A. Balmaseda, G. Balsamo, P. Bauer, P. Bechtold, A.C.M. Beljaars, L. van de Berg, J. Bidlot, N. Bormann, C. Delsol, R. Dragani, M. Fuentes, A.J. Geer, L. Haimberger, S.B. Healy, H. Hersbach, E.V. Hólm, L. Isaksen, P. Kållberg, M. Köhler, M. Matricardi, A.P. McNally, B.M. Monge-Sanz, J.-J. Morcrette, B.-K. Park, C. Peubey, P. de Rosnay, C. Tavolato, J.-N. Thépaut, and F. Vitart. The era-interim reanalysis: configuration and performance of the data assimilation system. *Quarterly Journal of the Royal Meteorological Society*, 137:553–597, 2011.
- [10] I. Epicoco, S. Mocavero, and G. Aloisio. Performance optimization of nemo oceanic model at high resolution. In *Geophysical Research Abstracts Vol. 16, EGU2014-4468, 2014, id. 4468, 2014.*
- [11] T. Fichefet and M.A. Morales Maqueda. Sensitivity of a global sea ice model to the treatment of ice thermodynamics and dynamics. *Journal of Geophysical Research*, 102:12609–12646, 1997.
- [12] P. Fretwell, H.D. Pritchard, D.G. Vaughan, J.L. Bamber, N.E. Barrand, R. Bell, C. Bianchi, R.G. Bingham, D.D. Blankenship, G. Casassa, G. Catania, D. Callens, H. Conway, A.J. Cook, H.F.J. Corr, D. Damaske, V. Damm, F. Ferraccioli, R. Forsberg, S. Fujita, Y. Gim, P. Gogineni, J.A. Griggs, R.C.A. Hindmarsh, P. Holmlund, J.W. Holt, R. W. Jacobel, A. Jenkins, W. Jokar, T. Jordan, E.C.



- King, J. Kohler, W. Krabill, M. Riger-Kusk, K.A. Langley, G. Leitchenkov, C. Leuschen, B.P. Luyendyk, K. Matsuoka, J. Mouginot, F.O. Nitsche, Y. Nog, O. Nost, S.V. Popov, E. Rignot, D.M. Rippin, A. Rivera, J. Roberts, N. Ross, M.J. Siegert, A.M. Smith, D. Steinhage, M. Studinger, B. Sun, B.K. Tinto, B.C. Welch, D. Wilson, D.A. Young, C. Xiangbin, and A. Zirizzotti. Bedmap2: improved ice bed, surface and thickness datasets for antarctica. *The Cryosphere*, 7:375–393, 2013.
- [13] Retrieved from <https://climatedataguide.ucar.edu/climate-data/rapid-monitoring-atlantic-meridional-overturning-circulation> 265 The climate data guide: Rapid: monitoring the atlantic meridional overturning circulation at 26.5 °n., last modified 31 Oct 2013.
- [14] Kui Gao, Chen Jin, Alok Choudhary, and Wei keng Liao. Supporting computational data model representation with high-performance i/o in parallel netcdf. *EEE International Conference on High Performance Computing*, December 2011.
- [15] P. Gaspar, Y. Gregoris, and J.M. Lefevre. A simple eddy kinetic energy model for simulations of the oceanic vertical mixing: tests at station papa and long-term upper ocean study site. *Journal of Geophysical Research*, 95:16179–16193, 1990.
- [16] S.A. Good, M.J. Martin, and N.A. Rayner. En4: quality controlled ocean temperature and salinity profiles and monthly objective analyses with uncertainty estimates. *Journal of Geophysical Research: Oceans*, 118:6704–6716, 2013.
- [17] Goosse H. and T. Fichefet. Importance of ice-ocean interactions for the global ocean circulation: a model study. *Journal of Geophysical Research*, 104:23337–23355, 1999.
- [18] Robert Hallberg. Using a resolution function to regulate parameterizations of oceanic mesoscale eddy effects. *Ocean Modelling*, 72:92–103, 2013.
- [19] E.C. Hunke and J.K. Dukowicz. An elastic–viscous–plastic model for sea ice dynamics an elastic–viscous–plastic model for sea ice dynamics an elastic–viscous–plastic model for sea ice dynamics. *Journal of Physical Oceanography*, 27:1849–1867, 1997.
- [20] IHO IOC and BODC. Centenary edition of the gebco digital atlas, published on cd-rom on behalf of the intergovernmental oceanographic commission and the international hydrographic organization as part of the general bathymetric chart of the oceans, british oceanographic data centre, liverpool, u.k., 2003.
- [21] D. Iovino, M. Vancoppenolle, and T. Fichefet. Implementation of lim sea ice model in the cmcc global ocean high-resolution configuration. Technical report, Research Papers Issue RP0209, 2013.
- [22] D.R. Jackett and T. J. McDougall. Minimal adjustment of hydrographic data to achieve static stability. *Journal of Atmospheric and Oceanic Technology*, 12:381–389, 1995.
- [23] M. Jakobsson, N. Cherkis, J. Woodward, B. Coakley, and R. Macnab. A new grid of arctic bathymetry: A significant resource for scientists and mapmakers. *American Geophysical Union, EOS Transactions*, 81(9), 2000.
- [24] W.G. Large and S.G. Yeager. Diurnal to decadal global forcing for ocean and sea-ice models: the data sets and flux climatologies. Technical Report NCAR/TN-460+STR, CGD Division of the National Centre for Atmospheric Research (NCAR), 2004.



- [25] M. Lengaigne, C. Menkes, O. Aumont, T. Gorgues, L. Bopp, J.-M. Andre, and G. Madec. Bio-physical feedbacks on the tropical pacific climate in a coupled general circulation model. *Climate Dynamics*, 28:503–516, 2007.
- [26] Jianwei Li, Wei keng Liao, Alok Choudhary, Robert Ross, Rajeev Thakur, William Gropp, Rob Latham, Andrew Siegel, Brad Gallagher, and Michael Zingale. Parallel netcdf: A high-performance scientific i/o interface. *SC Conference*, page 39, 2003.
- [27] Jianwei Li, Wei keng Liao, Alok Choudhary, Robert Ross, Rajeev Thakur, William Gropp, Rob Latham, Andrew Siegel, Brad Gallagher, and Michael Zingale. Parallel netcdf: A scientific high-performance i/o interface. *Proceedings of Supercomputing Conference*, November 2003.
- [28] R.A. Locarnini, A.V. Mishonov, J.I. Antonov, T.P. Boyer, H.E. Garcia, O.K. Baranova, M.M. Zweng, C.R. Paver, J.R. Reagan, D.R. Johnson, M. Hamilton, and D. Seidov. *World Ocean Atlas 2013, Volume 1: Temperature*. S. Levitus, Ed., A. Mishonov Technical Ed.; NOAA Atlas NESDIS 73, 40 pp., 2013.
- [29] G. Madec, P. Delecluse, M. Imbard, and C. Lévy. Opa 8.1 ocean general circulation model reference manual. Technical report, Note du Pôle de modélisation, Institut Pierre-Simon Laplace, N°11, 91, pp., 1998.
- [30] Gurvan Madec and the NEMO team. Nemo ocean engine – Version 3.4. Technical Report ISSN No 1288–1619, Pole de modelisation de l’Institut Pierre-Simon Laplace No 27, 2012.
- [31] A. J. G. Nurser and S. Bacon. The rossby radius in the arctic ocean. *Ocean Science*, 10:967–975, 2014.
- [32] U.S. Department of Commerce, National Oceanic and Atmospheric Administration, and National Geophysical Data Center. 2-minute Gridded Global Relief Data (ETOPO2v2). <http://www.ngdc.noaa.gov/mgg/fliers/06mgg01.html>, 2006.
- [33] Rodgers David P. Improvements in multi-processor system design. *IEEE, Computer Society Press Los Alamitos*, 1985.
- [34] Morrow R. and P.-Y. Le Traon. Recent advances in observing mesoscale ocean dynamics with satellite altimetry. *Advances in Space Research*, 50(8):1062–1076, 2012.
- [35] R.W. Reynolds, T.M. Smith, C. Liu, D.B. Chelton, K.S. Casey, and M. G. Schlax. Daily high-resolution blended analyses for sea surface temperature. *Journal of Climate*, 20:5473–5496, 2007.
- [36] R.D. Smith, M.E. Maltrud, F. Bryan, and M.W. Hecht. Numerical simulation of the north atlantic ocean at 1/10. *Journal of Physical Oceanography*, 30:1532–1561, 2000.
- [37] W. H. F Smith and D. T. Sandwell. Global seafloor topography from satellite altimetry and ship depth soundings. *Science*, 277(5):1956–1962, 1997.
- [38] A. Storto and S. Masina. The cmcc global ocean physical reanalysis system (c-glors) version 3.1: Configuration and basic validation. Technical report, Research Papers Issue RP0211, 2013.
- [39] M.M. Zweng, J.R. Reagan, J.I. Antonov, R.A. Locarnini, A.V. Mishonov, T.P. Boyer, H.E. Garcia, O.K. Baranova, D.R. Johnson, D. Seidov, and M.M. Biddle. *World Ocean Atlas 2013, Volume 2: Salinity*. S. Levitus, Ed., A. Mishonov Technical Ed.; NOAA Atlas NESDIS 74, 39 pp., 2013.



© **Centro Euro-Mediterraneo sui Cambiamenti Climatici 2015**
Visit www.cmcc.it for information on our activities and publications.

The Euro-Mediterranean Centre on Climate Change is a Ltd Company with its registered office and administration in Lecce and local units in Bologna, Venice, Capua, Sassari, Viterbo, Benevento and Milan. The society doesn't pursue profitable ends and aims to realize and manage the Centre, its promotion, and research coordination and different scientific and applied activities in the field of climate change study.

